Supplementary Legends

Supplementary Figure 1 Fibronectin and interstitial fluid localization at the neurectoderm-to-prechordal plate interface during zebrafish gastrulation.

(a, b, c) Immunofluorescence confocal images of the neurectoderm (ecto)-to-prechordal plate (ppl) interface (white dashed line) in a wild type (wt) embryos at 6 (a), 8 (b), and 9 (c) hpf showing Fibronectin staining (pseudo-colored with Fire LUT) in maximum intens ity projections of dorsal views (top panels) and sagittal sections (middle panels); red dashed line outlines position of ppl leading edge cells; blue dashed line indicates ecto-to-EVL interface, and yellow dashed line shows YSL interface to ppl and ecto; bottom panels are sagittal sections of the ecto-to-ppl interface stained for F-actin (phalloidin) to mark this interface; double-sided arrows indicate animal (A) to vegetal (V) and dorsal (V) to ventral (V) embryo axes; asterisk labels ppl leading edge cell; scale bar, 20 µm.

(d) Multiphoton live cell images showing interstitial fluid (IF) accumulation (dextran-Alexa Fluor 647, left panel), F-actin localization (*Tg*(*actb1:lifeact*-GFP), middle panel) and a combination of those different labels (right panel) at the ecto-to-ppl interface (white dashed line) at 7 hpf; red arrows indicate extracellular cavities filled with IF at the ecto-to-ppl and ecto-to-YSL interfaces; white arrows indicate ecto-to-ppl cell-cell contacts devoid of IF accumulations; blue dashed line indicates ecto-to-EVL interface, and yellow dashed line shows YSL interface to ppl and ecto; double-sided arrows indicate AV and dorsal DV embryo axes; asterisk labels ppl leading edge cell; scale bar, 20 µm.

(e) Multiphoton live cell image of *Tg(gsc:*GFP) embryo (t = 120 min, 8 hpf) with pseudo-colored spots marking positions of nuclei within the axial mesendoderm (green); dorsal view with double-sided arrows indicating AP to VP and left (L) to right (R) embryo axes; color-code indicates mean total cell speeds of axial mesendoderm cells moving to the animal pole after internalization (cyan, 0-2 and yellow/magenta >2 µm/min); position of anterior (ppl) and posterior mesendoderm marked; scale bar, 50 µm.

(f) Average instantaneous cell speeds in µm/min of internalized axial mesendoderm cells in wt embryos (n=6 embryos) plotted along the normalized distance along the AV axis from anterior (0) to posterior (1); green dashed line marks position of transition from anterior (ppl) to posterior axial mesendoderm, error bars, s.e.m.

Supplementary Figure 2 Prechordal plate and neurectoderm cell movements and neural plate positioning in wild type and MZ*oep* mutant embryos.

(a) Fluorescent images of a wild type (wt) *Tg(gsc:*GFP) embryo showing neurectoderm nuclei (H2A-BFP, cyan) and *gsc*-expressing GFP-labeled prechordal plate (ppl) cells at a representative time point during gastrulation (t = 65 min, 7.1 hpf); dorsal and sagittal (dorsal up) sections through the embryo (yellow tags in upper panel mark sagittal section plane in lower panel); animal (AP) and vegetal pole (VP) indicated by arrows; scale bar, 100 µm.

(b) Correlation of ppl cell movements in a wt embryo at a representative time point during gastrulation (t = 111.7 min, 7.9 hpf); ppl cells are visualized as arrows in a 2D plot and color-coded corresponding to their 3D correlation values between 1 (red, maximum correlation) and -1 (blue, minimum correlation); every 3rd cell is plotted; AP, animal pole; VP, vegetal pole; scale bar, 50 µm.

(c) Average degree of alignment of ppl cell movements in wt embryos (n=5 embryos) plotted from 6 to 8 hpf (120 min); the order parameter corresponds to the degree of alignment ranging from 0 (disordered movement) to 1 (highly ordered movement); error bars, s.e.m.

(d) Mean instantaneous cell speed and directionality of ppl cells in a wt embryo (n=5 embryos) calculated from 6 to 8 hpf are plotted as bar graphs; error bars, s.e.m.

(e) Schematic illustration of global neurectoderm velocity measurements at the dorsal side of the embryo; the neurectoderm was segmented into 100 x 200 µm sectors along the AV axis (V_{AV}); sectors were positioned and color-coded relative to the ppl leading edge (yellow dot), or fixed for cases without ppl cells; A1-3 and P1-3, sector anterior and posterior of the ppl leading edge, respectively; mean V_{AV} velocities in the different sectors were calculated for each time frame.

(f) Mean movement velocities (µm/min) along the AV axis (V_{AV}) of neurectoderm cells in wt embryos (n=6 embryos) plotted from 6 to 8 hpf (120 min); colors of curves correspond to respective sectors in (e); error bars, s.e.m.

(g) Schematic illustration of global 3D movement correlation analysis between neurectoderm and ppl cells in defined sectors along the AV axis of the embryo. For 3D correlation calculations, neurectoderm cell velocities along the AV (V_{AV}), left-right (LR) (V_{LR}; see (e)) and dorsal-ventral (DV) axis (V_{DV} in sectors of 130x100 µm) were measured; sectors were positioned and color-coded relative to the ppl leading

edge (yellow dot); A1-3 and P1-3, sector anterior and posterior of the ppl leading edge (yellow dot), respectively.

(h) 3D movement correlation between leading edge ppl and adjacent neurectoderm cells in defined sectors along the AV axis of wt embryos (n=6 embryos) plotted from 6 to 8 hpf (120 min); colors of curves correspond to respective sectors in (e) and (g); error bars, s.e.m.

(i) Fluorescent images of a MZ*oep;Tg(dharma:*EGFP*)* mutant embryo showing neurectoderm nuclei (H2A-BFP, cyan) and Dharma (*dharma:*EGFP, green, marked with asterisk) expression at the dorsal blastoderm margin at a representative time point during gastrulation (t = 74.22 min, 7.2 hpf); dorsal and sagittal (dorsal up) sections through the embryo (yellow tags in upper panel mark sagittal section plane in lower panel); animal (AP) and vegetal pole (VP) indicated by arrows; scale bar, 100 µm.

(j) Mean movement velocities (µm/min) of neurectoderm cells along the AV axis (V_{AV}) in MZ*oep* mutant embryos (n=4 embryos) plotted over from 6 to 8 hpf (120 min); colors of curves correspond to sectors outlined in (e); error bars, s.e.m.

(k, l) Anterior neural anlage in wt (k) and MZ*oep* mutant (l) embryos marked by whole-mount *in situ* hybridization of *otx2* mRNA expression at consecutive stages of gastrulation from 70% epiboly to bud stage (7 - 10hpf); posterior axial mesoderm was detected by *no tail (ntl)* mRNA expression (arrows); animal pole (dorsal down), dorsal (animal pole up) and lateral (dorsal right) views are shown; arrowheads mark the anterior most edge of the neural plate; scale bars 200 µm.

(m) Quantitative analysis of neural plate position during gastrulation in MZ*oep* versus wt embryos. The angle (°) between the vegetal pole and the anterior border of the *otx2* expression domain was measured for embryos at different stages during gastrulation (k, l) and plotted as box-whisker graphs; n, embryos analyzed from 4 independent experiments; student's t-test (*P* value indicated) for all graphs comparing same stages; ***, $P < 0.001$, (ns) non significant, $P > 0.05$; n (wt, bud) = 36, n (wt, 90%) = 36, n (wt, 80%) = 34, n (wt, 70%) = 29, n (MZ*oep*, bud; $P < 0.0001$) = 24, n (MZ*oep*, 90%; $P < 0.0001$) = 36, n (MZ*oep*, 80%; $P < 0.0001$) = 20, n (MZ*oep*, 70%; $P < 0.358$) = 18; box plot centre, median; red dot, mean; upper whisker, maximum; lower whisker, minimum.

Supplementary Figure 3 Prechordal plate cell movements and neural plate positioning in *cyc* and *slb* morphant embryos.

(a, e) Fluorescence images of a Tg(*gsc:*GFP) *cyclops (cyc)* (a) and *silberblick (slb)* morphant (e) embryo showing H2A-BFP expression (cyan) in all nuclei and GFP (green, white outline) expression in *gsc*-expressing prechordal plate (ppl) cells at a representative time point during gastrulation (a; t = 71.40 min, 7.2 hpf and e; t = 74.22 min, 7.2 hpf); dorsal and sagittal (dorsal up) sections through the embryo (yellow tags in upper panel mark sagittal section plane in lower panel); animal (AP) and vegetal pole (VP) indicated by arrows; red line in (e) indicates widened ppl internalization zone; scale bar, 100µm.

(b, f) Number of internalized ppl cells in *Tg(gsc:*GFP) *cyc* (b; blue curve, n = 3 embryos) and *slb* (f; blue curve, n = 3 embryos) morphant embryos (blue curve, n = 3 embryos) versus wt (green curve, n = 6 embryos) embryos plotted between 6 and 8 hpf (120 min); error bars, s.e.m.

(c, g) Average degree of alignment of ppl cell movements in *cyc* (c) magenta curve/squares, n = 3 embryos) and *slb* morphant (g; magenta curve/dots, n=3 embryos) versus wt (green curve/dots, see Supplementary Fig. 2c) embryos plotted from 6 to 8/8.3 hpf (120/140 min); the order parameter corresponds to the degree of alignment ranging from 0 (disordered movement) to 1 (highly ordered movement); error bars, s.e.m.

(d, h) Mean instantaneous ppl cell speed and directionality of *cyc* [d; gray bar graph, n = 4 embryos; *P(speed)* = 0.0061, *P(dir)* = 0.033] and *slb* morphant [gray bar graphs, n = 3 embryos, *P(speed)* = 0.0025, *P(dir)* <0.0001] versus wt (white bar graph, see Supplementary Fig. 2d) embryos plotted as bar graphs; error bars, s.e.m.; student's t-test for all graphs; ***, $p < 0.001$, **, $p < 0.01$; *, $p < 0.05$.

(i, j) Anterior neural plate anlage in *cyc* and *slb* morphant embryos marked by whole-mount in situ hybridization of *otx2* mRNA expression at consecutive stages of gastrulation from 70% epiboly to bud stage (7 - 10hpf); posterior axial mesoderm was detected by *no tail (ntl)* mRNA expression (arrows); animal pole (dorsal down), dorsal (animal pole up) and lateral (dorsal right) views are shown; arrowheads mark the most anterior edge of the neural plate; scale bar 200 µm.

(k) Quantitative analysis of neural plate position in *cyc* and *slb* morphant versus wt embryos during gastrulation. The angle (°) between the vegetal pole and the anterior border of the *otx2* expression domain was measured for embryos at different stages

during gastrulation (i, j) and plotted as box-whisker graphs; n, embryos analyzed from 4 independent experiments; student's t-test (*P* value indicated) for all graphs comparing same stages; ***, $P < 0.001$, ns (non significant), $P > 0.05$; n (wt, bud) = 36, n (wt, 90%) = 36, n (wt, 80%) = 34, n (wt, 70%) = 29, n (*slb*, bud; $P < 0.0001$) = 23, n (*slb*, 90%; $P < 0.0001$) = 17, n (*slb*, 80%; $P < 0.0001$) = 20, n (*slb*, 70%; $P = 0.134$) = 16, n (*cyc*, bud; $P < 0.0001$) = 40, n (*cyc*, 90%; $P < 0.0001$) = 39, n (*cyc*, 80%; $P < 0.0001$) = 32, n (*cyc*, 70%; $P = 0.851$) = 27; red dots mark mean values; box plot centre, median; red dot, mean; upper whisker, maximum; lower whisker, minimum.

Supplementary Figure 4 Prechordal plate cell movements and neural plate positioning in wild type embryos overexpressing CA-Mypt within the yolk syncytial layer.

(a) Schematic illustration of *CA-Mypt* and *H2A-mCherry* mRNA injection into the yolk syncytial layer (YSL) of an embryo at high stage (3.3 hpf).

(b) Confocal images of the enveloping layer (EVL)/YSL epiboly progression in F-actin labeled *Tg(actb1:*GFP-UtrCH*)* wild type (wt) control (lower panel) and embryos injected with constitutively active myosin II phosphatase mRNA into the YSL (CA-Mypt, upper panel) at 8 hpf; both embryos were co-injected with *H2A-mCherry* mRNA into the YSL to mark YSL nuclei.

(c) Quantification of the average advancement (µm/min) of the EVL margin of wt control and *CA-Mypt* injected embryos between 7 and 9 hpf; student's t-test; ***, $P < 0.001$; n= 4 embryos; error bars, s.e.m.

(d) Fluorescence images of a *Tg(gsc:*GFP*)* embryo overexpressing CA-Mypt and H2A-mCherry (magenta, arrows) within the YSL, also showing H2A-BFP expression within all nuclei and GFP-expression in *gsc*-expressing prechordal plate (ppl) progenitors (green, white outline) at a representative time point during gastrulation (t = 75 min, 6.25 hpf); dorsal and sagittal (dorsal up) sections through the embryo (yellow tags in upper panel mark sagittal section plane in lower panel); animal (AP) and vegetal pole (VP) indicated by arrows; scale bar, 100µm.

(e) Number of internalized ppl cells in *Tg(gsc:*GFP*)* embryos overexpressing CA-Mypt within the YSL (blue curve, n = 4 embryos) versus wt embryos (green curve) plotted from 6 to 8 hpf (120 min); error bars, s.e.m.

(f) Directional correlation of ppl cell movements in a wt embryo overexpressing CA-Mypt within the YSL at a representative time point during gastrulation (t = 77.40 min, 6.8 hpf); ppl cells are visualized as arrows in a 2D plot and color-coded according to their 3D correlation values between 1 (red, maximum correlation) and -1 (blue, minimum correlation); every 3rd cell is plotted; AP, animal pole; VP, vegetal pole; scale bar, 50 µm.

(g) Average degree of alignment of ppl movements in embryos overexpressing CA-Mypt within the YSL (magenta curve/squares, n = 3 embryos) versus wt embryos (green curve/dots, see Supplementary Fig. 1c) plotted from 6 to 8 hpf (120 min); the order parameter corresponds to the degree of alignment ranging from 0 (disordered movement) to 1 (highly ordered movement); error bars, s.e.m.

(h) Mean ppl cell instantaneous speed and directionality in CA-Mypt injected [gray bar graphs, n = 4 embryos; *P(speed)* = 0.323, *P(dir)* = 0.702] versus wt (white bar graphs, see Supplementary Fig. 2d) embryos plotted over 120min (6 to 8 hpf) as bar graphs; error bars, s.e.m.; student's t-test for all graphs; ns (not-significant), $P > 0.05$.

(i) Anterior neural anlage in embryos overexpressing CA-Mypt within the YSL marked by whole-mount *in situ* hybridization of *otx2* mRNA expression at consecutive stages of gastrulation from 70% epiboly to bud stage (7 - 10hpf); posterior axial mesoderm was detected by *no tail (ntl)* mRNA expression (yellow arrows); animal pole (dorsal down), dorsal (animal pole up) and lateral (dorsal right) views are shown; red arrowhead marks the most anterior edge of the neural plate; 200 µm.

(j) Quantitative analysis of neural plate position during gastrulation in embryos overexpressing CA-Mypt in the YSL versus wt embryos. The angle (°**)** between the vegetal pole and the anterior border of the otx2 expression domain was measured for embryos at different stages during gastrulation (i) and plotted as box-whisker graphs; n, embryos analyzed from 4 independent experiments; student's t-test (*P* value indicated) for all graphs comparing same stages; **, $P < 0.01$; *, $P < 0.05$, (ns) non significant, $P > 0.05$; n (wt, bud) = 36, n (wt, 90%) = 36, n (wt, 70%) = 29, n (CA-Mypt, bud; $P = 0.49$) = 16, n (CA-Mypt, 90%; $P = 0.0259$) = 22, n (CA-Mypt, 80%; $P = 0.0016$) = 34, n (CA-Mypt, 70%; $P = 0.0016$) = 12; red dots mark mean values; box plot centre, median; red dot, mean; upper whisker, maximum; lower whisker, minimum.

Supplementary Figure 5 Movement of transplanted prechordal plate cells in MZ*oep* mutant embryos.

(a, h) Schematic illustration of a MZ*oep*;*Tg(dharma:*EGFP*)* (a) and a MZ*oep*;*Tg(dharma:*EGFP*)* mutant embryo that was injected with *CA-Mypt* mRNA into the YSL at high stage (h; 3.3 hpf) transplanted with prechordal plate (ppl) cells (green) into the dorsal side at 60% epiboly (6 hpf); asterisk marks position of dorsal marker Dharma; orange arrows indicate reduced vegetal-directed movement of EVL margin (h); AP, animal pole; VP, vegetal pole; L, left; R, right.

(b, i) Bright-field/fluorescence image of a MZ*oep*;*Tg(dharma:*EGFP*)* mutant embryo at 90% epiboly (9 hpf) and a MZ*oep*;*Tg(dharma:*EGFP*)* mutant embryo at 80 % epiboly (8 hpf) that overexpresses CA-Mypt and the nuclei marker H2A-mCherry (red) within the YSL containing transplanted GFP-labeled ppl cells from *Tg(gsc*:GFP*)* donor (b) and *Tg(gsc*:GFP-CAAX*)* donor (i) embryos; ppl cell nuclei are marked by H2A-mCherry (i; red, co-localizes with green ppl cells); dashed white line indicates position of transplanted ppl progenitors; arrowhead points at anterior edge of ppl cells; asterisk marks *dharma*:EGFP signal at the dorsal side of the embryo; dorsal (animal pole up, top panel) and lateral (dorsal right, bottom panel) views; scale bar, 200 µm.

(c, j) Fluorescence images of representative time points during gastrulation (c; t = 47.19 min, 6.8 hpf and j; t = 56.39 min, 6.9 hpf) showing a MZ*oep*;*Tg(dharma:*EGFP*)* (c) and a MZ*oep*;*Tg(dharma:*EGFP*)* mutant embryo which overexpresses CA-Mypt and the nuclei marker H2A-mCherry (magenta) within the YSL (j) containing transplanted *gsc*-expressing GFP-labeled ppl cells (white outline) from *Tg(gsc*:GFP*)* donor (c) and *Tg(gsc*:GFP-CAAX*)* donor (j) embryos; all nuclei are marked by H2A-mCherry (c; magenta) and H2A-BFP (j; cyan) expression, and the dorsal side of the embryos is marked by *dharma*:EGFP expression (green, asterisk); dorsal and sagittal (dorsal up) sections through the embryo (yellow tags in upper panel mark sagittal section plane in lower panel); animal pole (AP) and vegetal pole (VP) indicated by arrows; scale bar, 100µm.

(d) Protrusion orientation of ppl cells transplanted into MZ*oep* mutants: top panel, fluorescence image of ppl cells with cytoplasm in green (*gsc*:GFP) and nuclei in cyan (H2A-BFP); animal pole up; scale bar, 20 µm. Bottom panel, polar plot or protrusion orientation of transplanted ppl cells (n = 48 cells from 2 embryos) with 0 ° = animal pole, 180 ° = vegetal pole.

(e) Number of ppl cells transplanted into MZ*oep* mutant embryos (n=3 embryos) plotted from 6 to 8 hpf (120 min); error bars, s.e.m.

(f) Directional correlation of transplanted ppl cell movements in a MZ*oep* mutant embryo at a representative time point during gastrulation (t = 83.5 min, 7.4 hpf); ppl cells are visualized as arrows in a 2D plot and color-coded according to their 3D correlation values between 1 (red, maximum correlation) and -1 (blue, minimum correlation); every 5th cell is plotted; AP, animal pole; VP, vegetal pole; scale bar, 50 µm.

(g) Average degree of alignment of transplanted ppl cell movements in MZ*oep* mutant embryos (magenta curve/squares, n=3 embryos) versus endogenous ppl cell movements in wt embryos (green curve/dots, see Supplementary Fig. 2c) from 6 to 8 hpf (120 min); the order parameter corresponds to the degree of alignment ranging from 0 (disordered movement) to 1 (highly ordered movement); error bars, s.e.m.

(k) Mean neurectoderm cell velocities along the animal-vegetal (AV) axis (V_{AV}) (measurement area indicated by black box in Supplementary Fig. 2e) in MZ*oep* mutant embryos (red curve, n=3 embryos) and MZ*oep* mutant embryos overexpressing CA-Mypt in the YSL (black curve, n=3 embryos); error bars, s.e.m.

Supplementary Figure 6 Effect of external friction on one-dimensional neurectoderm flow profile.

(a) For capturing the flow profile induced solely by prechordal plate (ppl) cells, MZ*oep* mutants devoid of ppl cells were used to measure unperturbed epiboly movements, and those movements were subtracted from the overall neurectoderm flow field in wt embryos. This allowed decomposing the neurectoderm flow field and obtaining the ppl-induced movement alterations only. In the 2D description, neurectoderm flows exclusively within the experimental image plane (red square) were taken into account.

(b) Theoretical 1D flow profile when the external friction coefficient ξ_0 between neurectoderm and tissues other than the ppl, such as the yolk cell and/or EVL, is varied. In case the external friction coefficient is increased, the range of flow triggered by ppl cells is decreased (blue: $\xi_0/\bar{\eta} = 10^{-11}\mu\mathrm{m}^{-2}$, orange: $\xi_0/\bar{\eta} = 10^{-5}\mu\mathrm{m}^{-2}$, green: $\xi_0/\bar{\eta} = 10^{-4}\mu\mathrm{m}^{-2}$, all curves: $f/\bar{\eta} = -4.2 \cdot 10^{-5}\mu\mathrm{m}^{-1} \cdot \mathrm{min}^{-1}$).

(c) Experimental velocities in wt embryos (blue dots) compared to theoretical flow profiles for the parameter settings as used in Fig. 5 (red dotted line, $f/\bar{\eta} = -4.2 \cdot 10^{-5}\mu\mathrm{m}^{-1} \cdot \mathrm{min}^{-1}, \xi_0/\bar{\eta} = 1.6 \cdot 10^{-6}\mu\mathrm{m}^{-2}$), and for zero external friction (green line, $f/\bar{\eta} = -3.5 \cdot 10^{-5}\mu\mathrm{m}^{-1} \cdot \mathrm{min}^{-1}, \xi_0/\bar{\eta} = 0$). The experimental velocity profile in wt embryos is well explained by either a small ($\xi_0 < \bar{\eta}/{L_E}^2$) or vanishing ($\xi_0$ =0) external friction coefficient.

Supplementary Figure 7 Prechordal plate cell movements and neural plate positioning in *e-cadherin* morphant embryos.

(a) Brightfield/fluorescence image of a wild type (wt) *Tg(gsc:*GFP*)* (top panel) and *e-cadherin* (*e-cad*) morphant embryo (bottom panel) with *gsc*-expressing GFP-labeled prechordal plate progenitor (ppl) cells (green, white outline) at 80% epiboly; dorsal views, animal pole up; the increasing distance between the margins of the enveloping layer (EVL; red dashed line) and deep cell/neurectoderm (blue dashed line) shows (neur)ectoderm epiboly delay in *e-cad* morphant embryos; scale bar, 200 µm.

(b) Fluorescence images of a *Tg(gsc:*GFP*) e-cad* morphant embryo showing H2A-mCherry (magenta) expression in all nuclei and GFP (green) expression in ppl cells (white outline) at a representative time point during gastrulation (t = 80.30 min, 7.3 hpf); dorsal and sagittal (dorsal up) sections through the embryo (yellow tags in upper panel mark sagittal section plane in lower panel); red and blue dashed lines as in (A); animal pole (AP) and vegetal pole (VP) indicated by arrows; scale bar, 100 µm.

(c) Number of internalized ppl cells in *Tg(gsc:*GFP*) e-cad* morphant (blue curve, n=4 embryos) versus wt (green curve) embryos plotted from 6 to 8 hpf (120 min); error bars, s.e.m.

(d) Correlation of ppl cell movements in a *e-cad* morphant embryo at a representative time point during gastrulation (t = 80 min, 7.3 hpf); ppl cells are visualized as arrows in a 2D plot and color-coded according to their 3D correlation values between 1 (red, maximum correlation) and -1 (blue, minimum correlation); every 3rd cell is plotted; AP, animal pole; VP, vegetal pole; scale bar, 50 µm.

(e) Average degree of alignment of ppl movements in *e-cad* morphant (magenta curve/squares, n=3) versus wt (green curve/dots, see Supplementary Fig. 2c) embryos from 6 to 8 hpf (120 min); the order parameter corresponds to the degree of alignment, ranging from 0 (disordered movement) to 1 (highly ordered movement); error bars, s.e.m.

(f) Mean ppl instantaneous speed and directionality in *e-cad* morphant [gray bar graphs, n=4 embryos; *P(speed)* = 0.0362; *P(dir)* = 0.222] versus wt (white bar graphs, see Supplementary Fig. 2d) embryos plotted as bar graphs; error bars, s.e.m; student's t-test for all graphs; *, $P < 0.05$; (ns) non significant, $P > 0.05$.

(g) Model of friction generation under E-cadherin reduced conditions (compare with wt in Fig. 6f) in *e-cadherin* morphant embryo leads to decreased friction at the ppl-to-neurectoderm (ecto) interface and to non-graded velocities within the ppl (left panel;

F_f, friction force; orange dashes indicate remaining cadherin); reduced E-cadherin-mediated adhesion between ppl and neurectoderm leads to loss of frictional drag and vegetal-directed movements (red arrow) of neurectoderm cells (right panel; yellow arrows indicate ppl movement); double-sided arrows indicate embryonic axes, animal (A) to vegetal (V), dorsal (D) to ventral (V).

(h) 2D tissue flow map indicating velocities (µm/min) of neurectoderm (ectoderm) cell movements along the AV (V_{AP}) and left-right (LR) (V_{LR}) axis at the dorsal side of a MZ*oep* embryo overexpressing CA-Mypt within the YSL and transplanted with *e-cad* morphant ppl cells (t = 41.40 min, 6.7 hpf) at a representative time point; average velocity vector for each defined area is indicated and color-coded ranging from 0 (blue) to 2 (red) µm/min; positions of all/leading edge ppl cells are marked by black/green dots; black boxed area was used for mean velocity measurements in (i); scale bar, 100 µm.

(i) Mean movement velocities (µm/min) along the AV axis (V_{AV}) of ppl leading edge progenitor cells (green curve, left y-axis) and neurectoderm (ecto) cells positioned above the ppl leading edge (black boxed area in h; red curve, right y-axis) in MZ*oep* embryos overexpressing CA-Mypt within the YSL and transplanted with *e-cad* morphant ppl cells (n=4 embryos) plotted from 6 to 8 hpf; vertical dashed line indicates start of vegetal-directed movements of ppl cells; error bars, s.e.m.

(j) 3D directional correlation values between leading edge ppl and adjacent neurectoderm (ecto) cells in MZ*oep* embryo overexpressing CA-Mypt within the YSL and transplanted with *e-cad* morphant ppl cells (t = 41.40 min, 6.7 hpf) at a representative time point during gastrulation; degree of correlation is color-coded ranging rom 1 (red, highest) to -1 (white, lowest); average neurectoderm velocities for each defined area are marked; black boxed area was used for local correlation measurements in (k); scale bar, 100 µm.

(k) 3D directional correlation values between leading edge ppl and adjacent neurectoderm (ecto) cells (black boxed area in j) in MZ*oep* embryos overexpressing CA-Mypt within the YSL and transplanted with *e-cad* morphant ppl cells (n=4 embryos) plotted from 6 to 8 hpf; error bars, s.e.m.

(l) Anterior neural anlage in *e-cad* morphant embryos marked by whole-mount *in situ* hybridization of *otx2* mRNA expression at consecutive stage during gastrulation from 70% to 90% epiboly (7 - 9hpf); posterior axial mesoderm was detected by *no tail (ntl)* mRNA expression (yellow arrows), animal pole (dorsal down), dorsal (animal pole

up) and lateral (dorsal right) views are shown; red arrowheads mark the most anterior edge of the neural plate; scale bar, 200 µm.

(m) Quantitative analysis of neural plate position during gastrulation in *e-cad* morphant versus wt embryos; the angle (°) between the vegetal pole and the anterior border of the *otx2* expression domain was measured for embryos at different stages (l) and plotted as box-whisker graphs; n, embryos analyzed from 4 independent experiments; student's t-test (*P* value indicated) for all graphs comparing same stages; ***, $P < 0.001$, (ns) non significant, $P > 0.05$; n (wt, 90%) = 36, n (wt, 80%) = 34, n (wt, 70%) = 29, n (*e-cad*, 90%; $P < 0.0001$) = 30, n (*e-cad*, 80%; $P < 0.0001$) = 37, n (*e-cad*, 70%; $P = 0.00036$) = 41; box plot centre, median; red dot, mean; upper whisker, maximum; lower whisker, minimum.

Supplementary Figure 8 Alterations in ectoderm movements upon application of E-cadherin mediated friction *ex vivo* and shear-strain-induced neurectoderm tissue deformation *in vivo*.

(a) Bright-field/fluorescence image showing setup of magnetic polystyrene beads (20 µm diameter) and fluorescent reference beads (red, 4 µm diameter) attached to a glass plate used to apply friction onto ectoderm cells; dashed line outlines shape of polystyrene cluster; scale bars, 100 µm and 20 µm for magnified area.

(b) Western Blot analysis showing detection of E-cadherin ectodomain (80 kDa) eluted from magnetic polystyrene beads coupled to E-cadherin-Fc Chimera (E-Fc) or uncoated control beads; molecular weight markers, 100 and 200 kDa.

(c) Section of maximum projection confocal image (see Fig. 7a; t = 19.33 min) showing top plate with fluorescent reference beads and selected beads are highlighted (red arrows in xy and yz cross-section); cross-section (yz; red rectangle) shows the position of E-Fc-coated beads (outlined in orange) at the ectoderm cell interface (yellow dashed line); direction of beads movement (top plate; - y; velocity ~ 1.5 µm/min) is indicated; scale bars, 100µm in xy and 20 µm in yz.

(d) Shear strain-induced neurectoderm tissue deformations of wild type (wt, upper panels; n=3 embryos) and MZ*oep* (lower panels; n=3 embryos) embryos plotted as time-averaged strain values for each domain (50 x 50 µm); average shear strain rate is color-coded according to amount of plane distortion [minimum green (0) to maximum red (5 $x10^{-3}s^{-1}$)]; tissue flows of neurectoderm are indicated as time-averaged velocities; dashed line indicates ppl and black dot marks ppl leading edge as reference point in wt and MZ*oep*; rectangle outlines area used for defining sectors along the animal-vegetal (AV) axis in (e).

(e) Mean shear strain rates of neurectoderm tissue of wt (upper panels; n=3 embryos) and MZ*oep* (lower panels; n=3 embryos) in defined sectors (100 x 200 µm) are plotted along the AV axis over time of gastrulation (plotted from 6.3 to 7.3 hpf in 10 min intervals); sectors were positioned and color-coded relative to the ppl leading edge (anterior A1-2 and posterior P1-2 of the ppl leading edge; for detailed description refer to Supplementary Fig. 1e); amount of plane distortion [minimum green (0) to maximum red (10 $x10^{-3}s^{-1}$)] is plotted along the y-axis;

(f) Neurectoderm tissue strain rate maps derived by subtraction of time-averaged shear strain values of wt from MZoep embryos (n=3 embryos); color-code as in (f);

tissue flows of neurectoderm are indicated as time-averaged velocities; dashed line indicates ppl and black dot marks ppl leading edge as reference point.

(g) Illustration of shear strain tissue deformation in the neurectoderm; arrows indicate direction of plane distortion of a tissue domain along the AV and left-right (LR) axis dependent on the direction and magnitude of neurectoderm movements; shear strain-induced domain angle of plane distortion can shrink (positive value) or enlarge (negative value).

Supplementary Video Legends

Supplementary Video 1 Live cell imaging of cell movements in wt embryo. Multiphoton time-lapse imaging of a wild type (wt) *Tg*(*gsc:*GFP) embryo with *gsc*-expressing GFP-labeled prechordal plate progenitor (ppl) cells (green) and neurectoderm cells at the dorsal side of the embryo from 6 to 8 hpf (123 min); all nuclei were labeled with histone H2A-BFP; animal/vegetal pole, up/down.

Supplementary Video 2 Life cell imaging of cell movements in MZ*oep* mutant embryo. Multiphoton time-lapse imaging of a MZ*oep*;*Tg*(*dharma*:EGFP) mutant embryo (Dharma:EGFP signal green) showing neurectoderm cells at the dorsal side of the embryo from 6 to 8.1 hpf (129 min); all nuclei were labeled with histone H2A-BFP; animal/vegetal pole, up/down.

Supplementary Video 3 2D velocities of neurectoderm cells in wt embryo. Tissue flow map indicating velocity vectors of neurectoderm cell movements along the animal-vegetal (AV) (V_{AV}) and left-right (LR) (V_{LR}) axis at the dorsal side of a wild type (wt) embryo between 6 to 8 hpf (117 min); average velocity vector for each defined area is indicated and color-coded ranging from 0 (blue) to 2 (red) µm/min; position of all/leading edge prechordal plate (ppl) cells are indicated as black/green dots; xy-axes in µm; time in mins; animal/vegetal pole, up/down.

Supplementary Video 4 3D correlation of neurectoderm and prechordal plate (pp) cell movements in wt embryo. Movement correlation between neurectoderm and underlying (ppl) cells at the dorsal side of a wild type (wt) embryo between 6 to 8 hpf (118 min); degree of correlation is color-coded ranging from 1 (red, highest correlation) to -1 (white, lowest correlation); average neurectoderm movement velocities and direction for each defined area are indicated by arrows; position of all/leading edge ppl cells are indicated as white/green dots; blue arrow marks movement direction of ppl leading edge cells; xy-axes in µm; time in mins; animal/vegetal pole, up/down.

Supplementary Video 5 2D velocities of neurectoderm cells in MZ*oep* mutant embryo. Tissue flow map indicating velocity vectors of neurectoderm cell

movements along the animal-vegetal (AV) (V_{AV}) and left-right (LR) (V_{LR}) axis at the dorsal side of a MZ*oep* mutant embryo between 6 to 8 hpf (121 min); average velocity vector for each defined area is indicated and color-coded ranging from 0 (blue) to 2 (red) µm/min; xy-axes in µm; time in mins; animal/vegetal pole, up/down.

Supplementary Video 6 3D correlation of neurectoderm and prechordal plate (pp) cell movements in *CA-Mypt* injected embryo. Movement correlation between neurectoderm and underlying prechordal plate (ppl) cells at the dorsal side of a wt embryo overexpressing CA-Mypt in the YSL between 6 to 8 hpf (118 min); degree of correlation is color-coded ranging from 1 (red, highest correlation) to -1 (white, lowest correlation); average neurectoderm movement velocities and direction for each defined area are indicated by arrows; position of all/leading edge ppl cells are indicated as white/green dots; blue arrow marks movement direction of ppl leading edge cells; xy-axes in µm; time in mins; animal/vegetal pole, up/down.

Supplementary Video 7 2D velocities of neurectoderm cells in ppl-transplanted MZ*oep* mutant embryo. Tissue flow map indicating velocity vectors of neurectoderm cell movements along the animal-vegetal (AV) (V_{AV}) and left-right (LR) (V_{LR}) axis at the dorsal side of a transplanted MZ*oep* mutant embryo between 6 to 7.5 hpf (91 min); average velocity vector for each defined area is indicated and color-coded ranging from 0 (blue) to 2 (red) µm/min; position of all/leading edge transplanted prechordal plate (ppl) cells are indicated as black /green dots; xy-axis in µm; time in mins; animal/vegetal pole, up/down.

Supplementary Video 8 2D velocities of neurectoderm cells in ppl-transplanted and *CA-Mypt* injected MZ*oep* mutant embryo. Tissue flow map indicating velocity vectors of neurectoderm cell movements along the animal-vegetal (AV) (V_{AV}) and left-right (LR) (V_{LR}) axis at the dorsal side of a MZ*oep* embryo overexpressing CA-Mypt within the YSL between 6 to 8 hpf (120 min); average velocity vector for each defined area is indicated and color-coded ranging from 0 (blue) to 2 (red) µm/min; position of all/leading edge transplanted prechordal plate (ppl) cells are indicated as black /green dots; xy-axis in µm; time in mins; animal/vegetal pole, up/down.

Supplementary Video 9 Arrangement of leading and trailing prechordal plate (ppl) cells in wild type (wt) embryo. Consecutive z-sections of a fluorescent imaging stack showing lifeact-GFP (F-actin) expressing ppl cells transplanted into the ppl leading edge of a wt embryo expressing Utrophin-mCherry (F-actin) and H2A-mCherry (nuclei); section starts at the ppl-neurectoderm interface and progresses through the leading edge ppl to the ppl-YSL interface; animal pole to the left; z-section taken from movie 16 at t = 12.36 min; scale bar, 20 µm.

Supplementary Video 10 Life cell imaging of leading and trailing prechordal plate (ppl) cells in wild type (wt) embryo. Fluorescence time-lapse imaging of lifeact-GFP (F-actin) expressing ppl cells transplanted into the ppl leading edge of a wt embryo expressing Utrophin-mCherry (F-actin) and H2A-mCherry (nuclei) starting at 70% epiboly (7 hpf); dorsal (top, animal pole left) and sagittal (bottom, animal pole left) sections through the embryo with dual (left side) and single (right side) color label; time in mins; scale bar, 20 µm.

Supplementary Video 11 2D velocities of neurectoderm cells in *e-cadherin* morphant embryo. Tissue flow map indicating velocity vectors of neurectoderm cell movements along the animal-vegetal (AV) (V_{AV}) and lefty-right (LR) (V_{LR}) axis at the dorsal side of a *e-cadherin* morphant embryo between 6 to 8 hpf (120 min); average velocity vector for each defined area is indicated and color-coded ranging from 0 (blue) to 2 (red) µm/min; position of all/leading edge prechordal plate (ppl) cells are indicated as black /green dots; xy-axis in µm; time in mins; animal/vegetal pole, up/down.

Supplementary Video 12 3D correlation of neurectoderm and prechordal plate (ppl) cell movements in *e-cadherin* morphant embryo. 3D movement correlation between neurectoderm and underlying prechordal plate (ppl) cells at the dorsal side of *e-cadherin* morphant embryo 6 to 8 hpf (120 min); degree of correlation is color-coded ranging from 1 (red, highest correlation) to -1 (white, lowest correlation); average neurectoderm movement velocities and direction for each defined area are indicated by arrows; position of all/leading edge ppl cells are indicated as white/green dots; blue arrow marks movement direction of ppl leading edge cells; xy-axes in µm; time in mins; animal/vegetal pole, up/down.

Supplementary Figure-1, Heisenberg

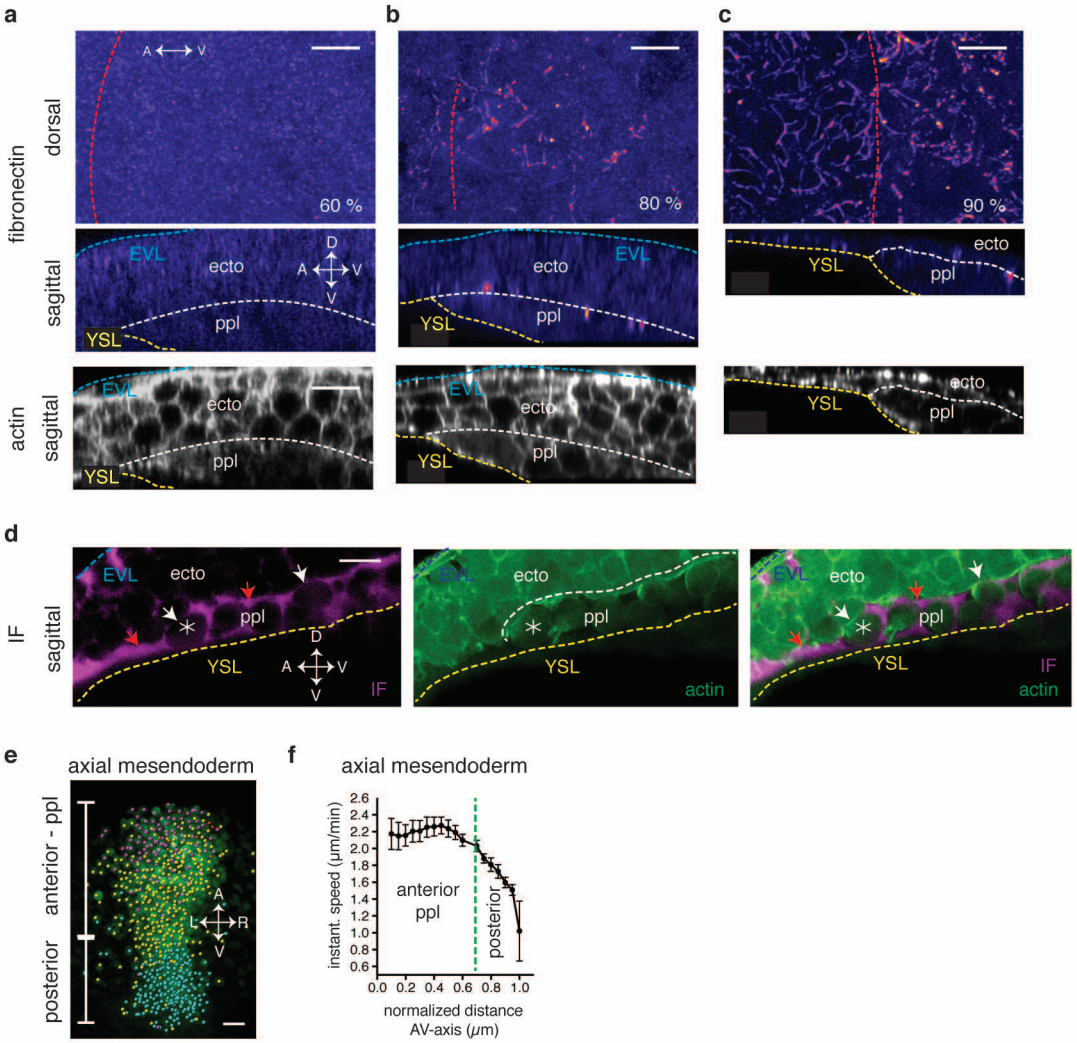

Supplementary Figure-2, Heisenberg

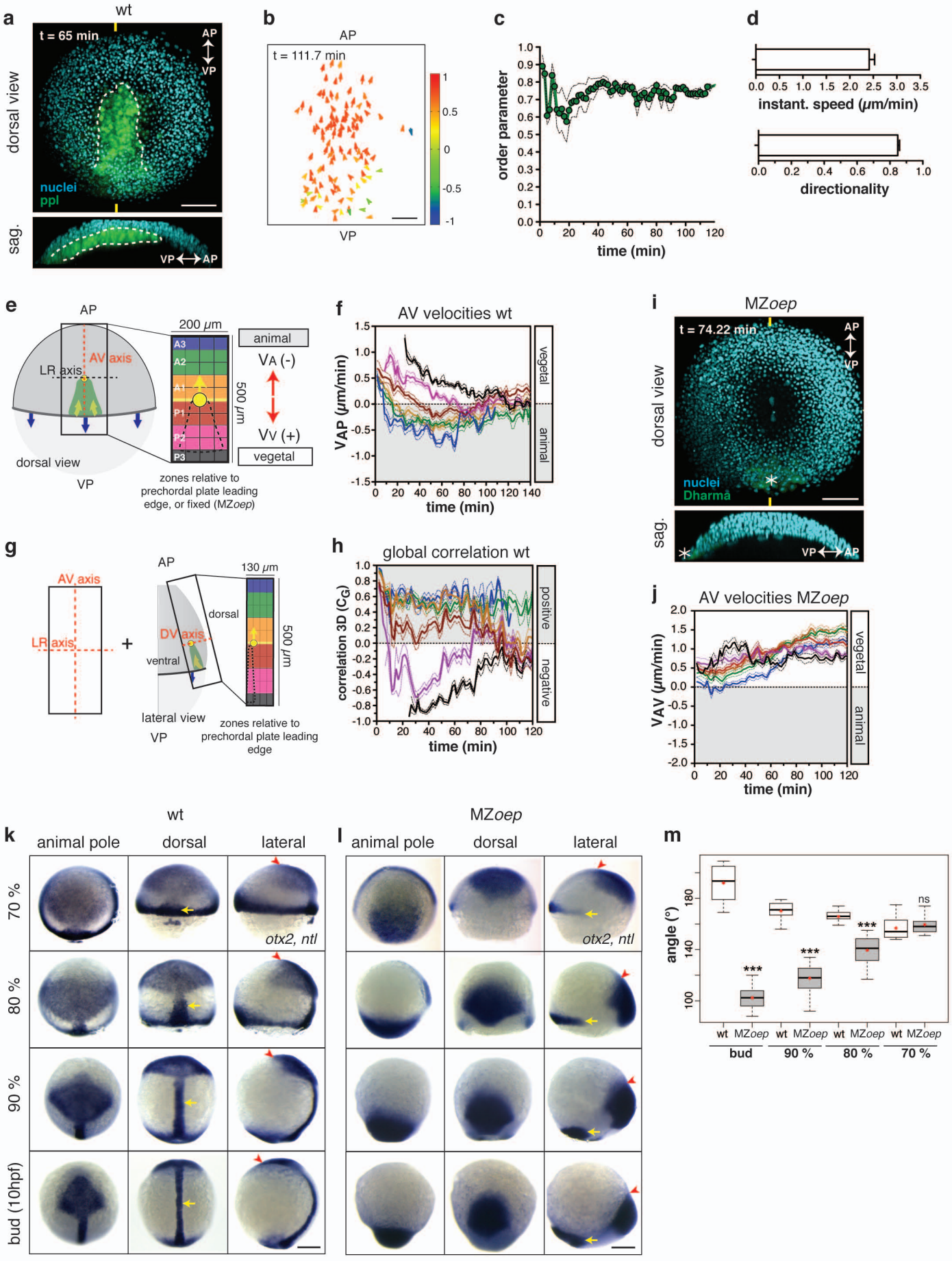

Supplementary Figure-3, Heisenberg

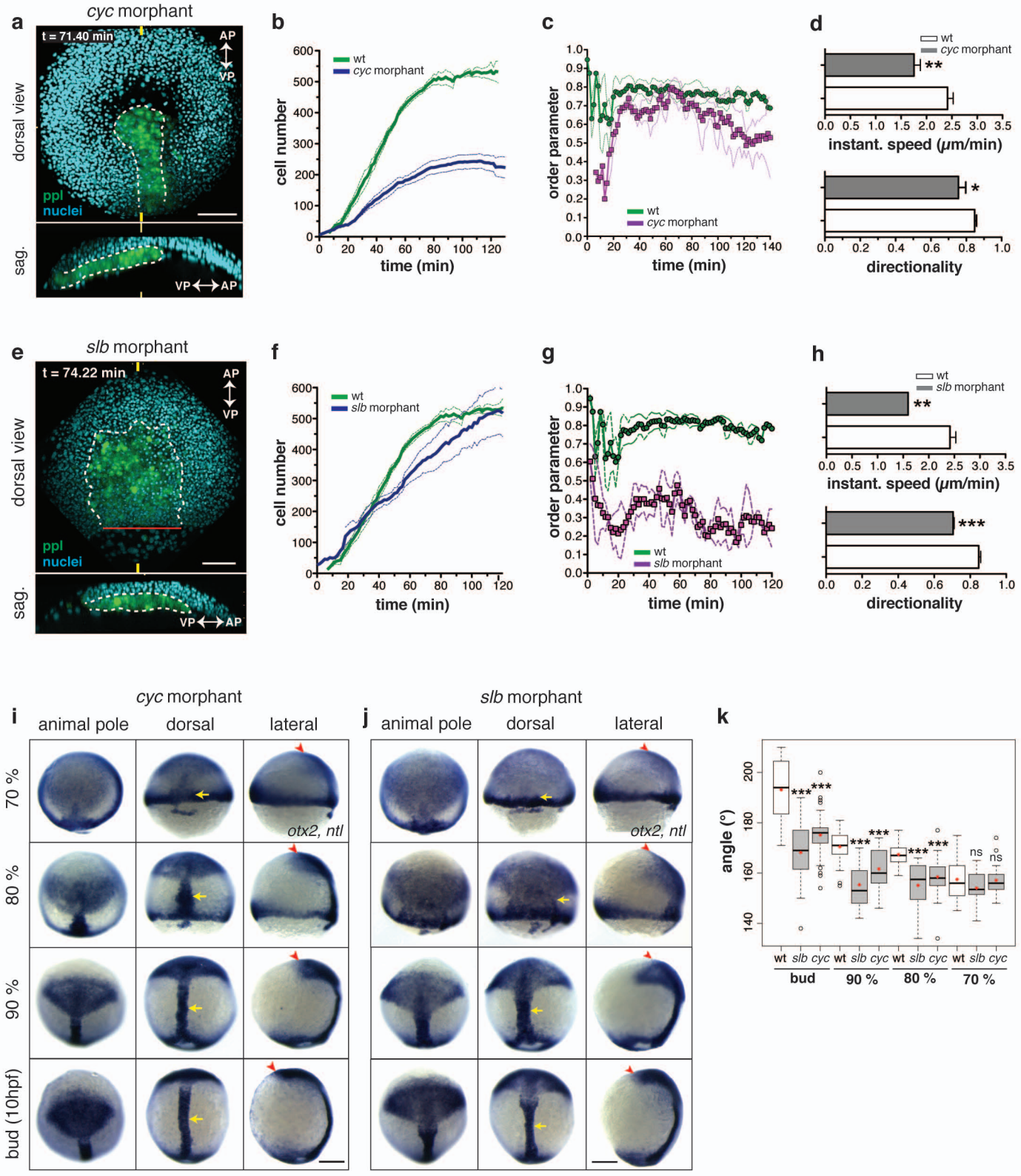

Supplementary Figure-4, Heisenberg

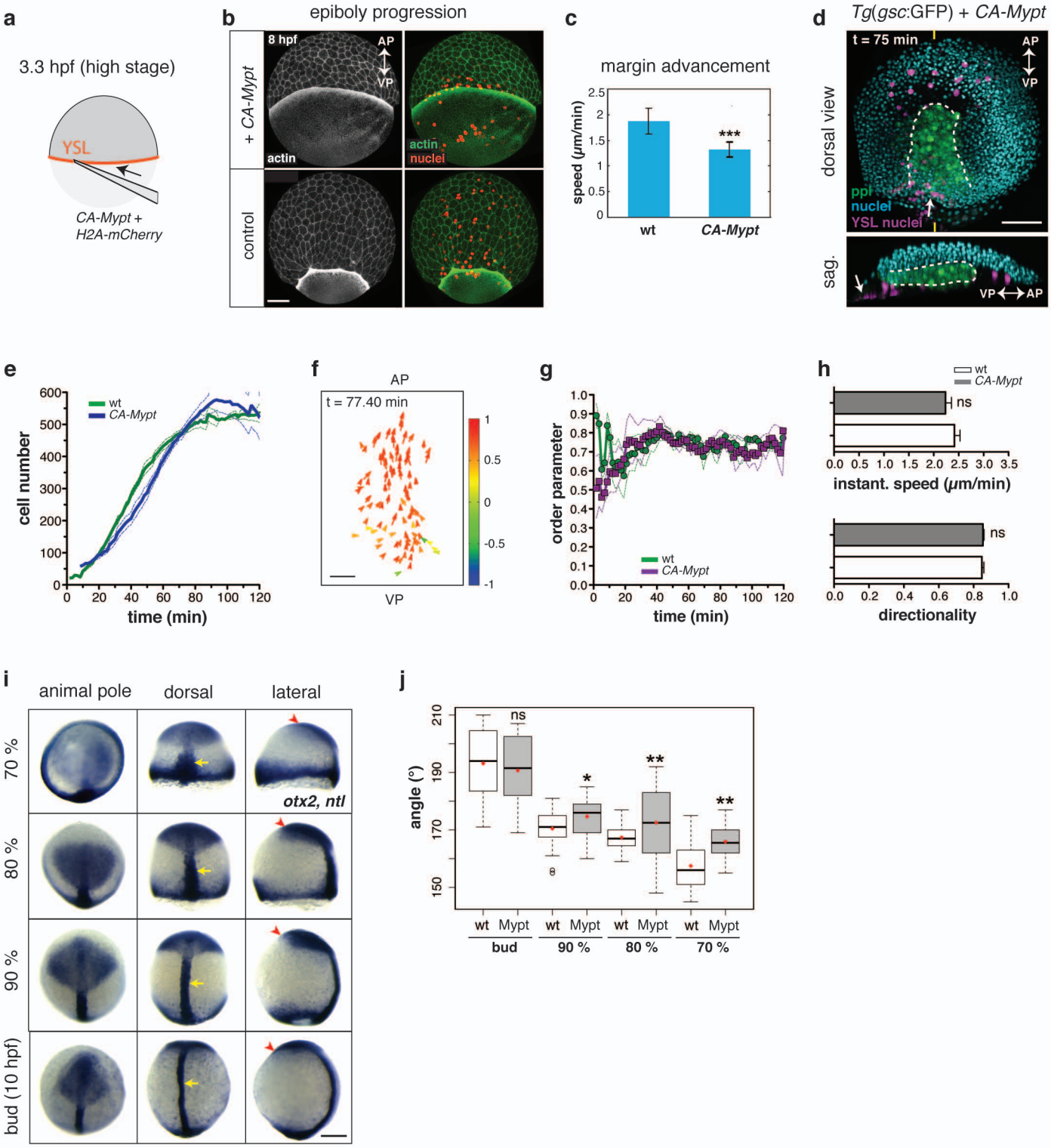

Supplementary Figure-5, Heisenberg

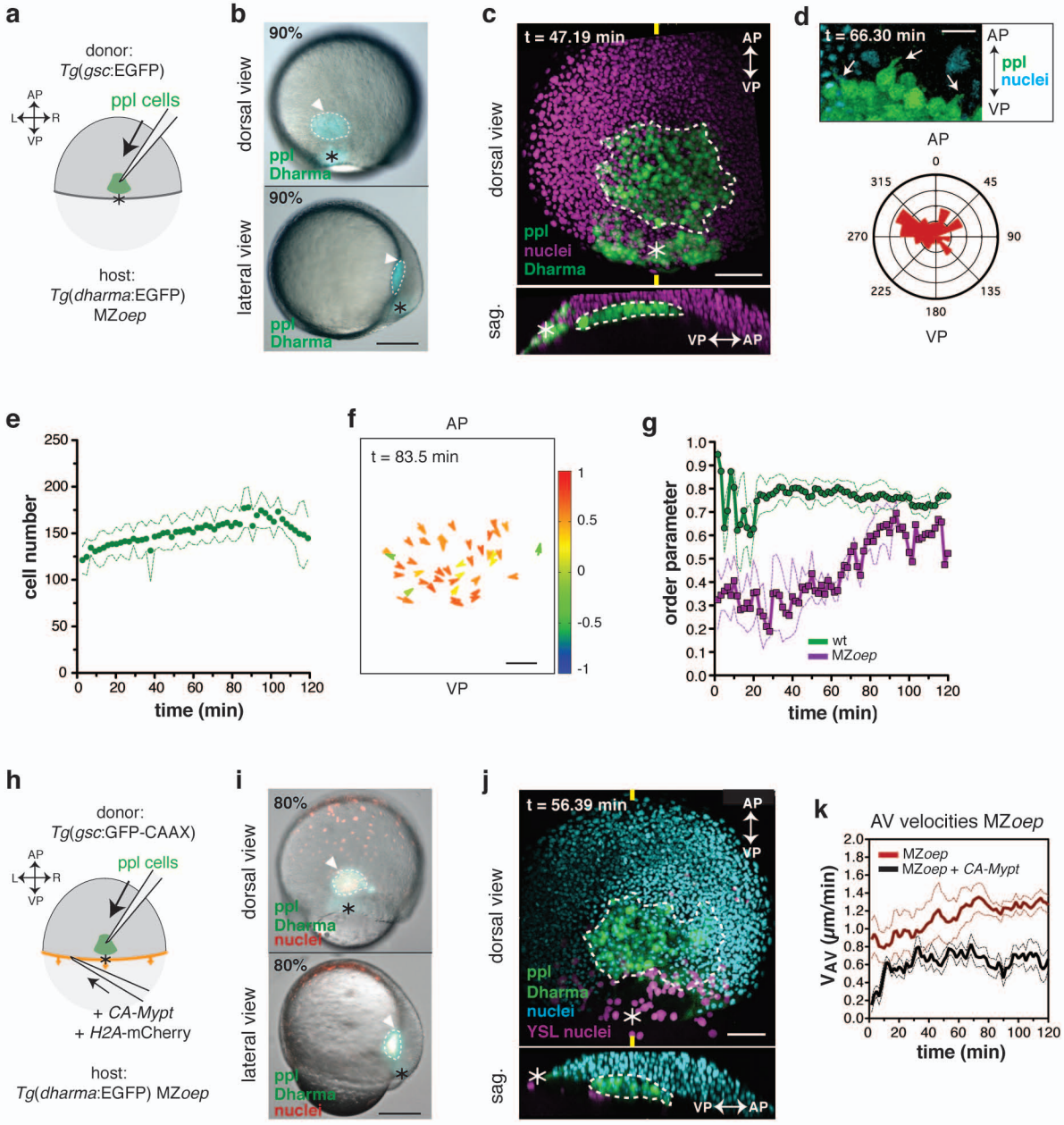

Supplementary Figure-6, Heisenberg

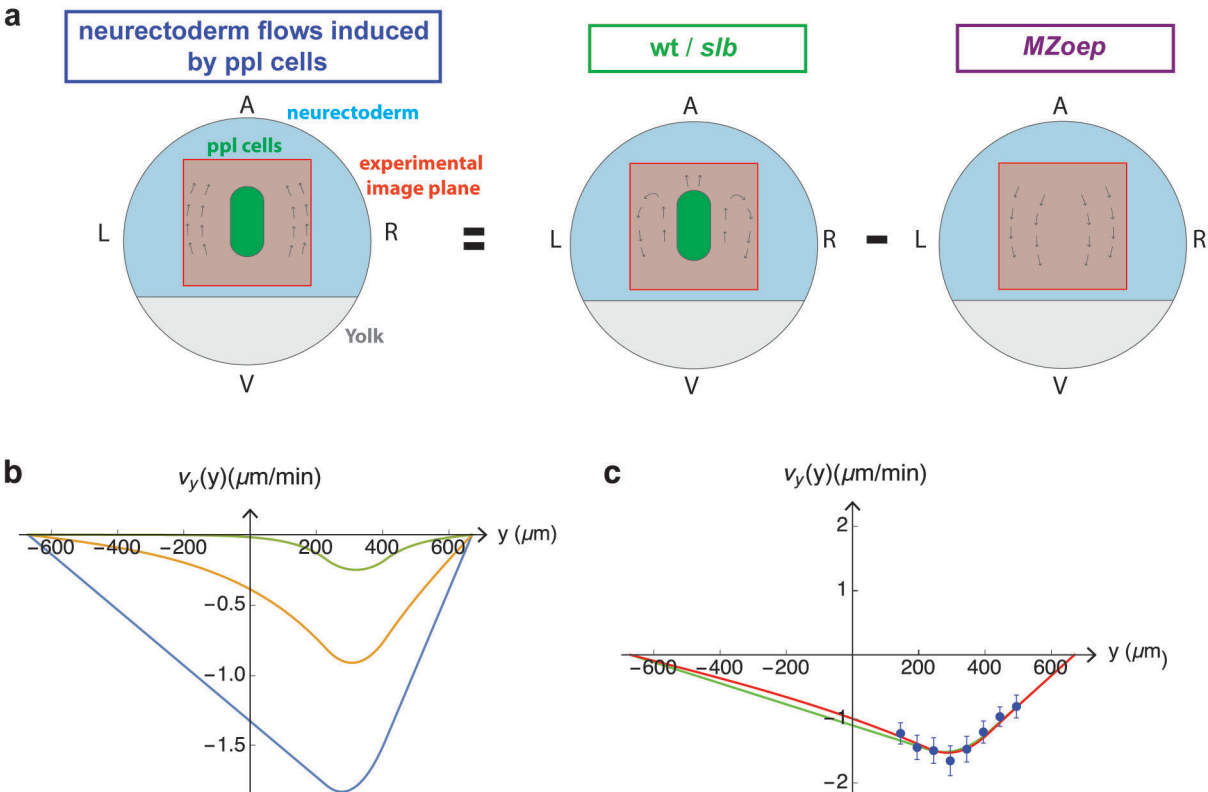

Supplementary Figure-7, Heisenberg

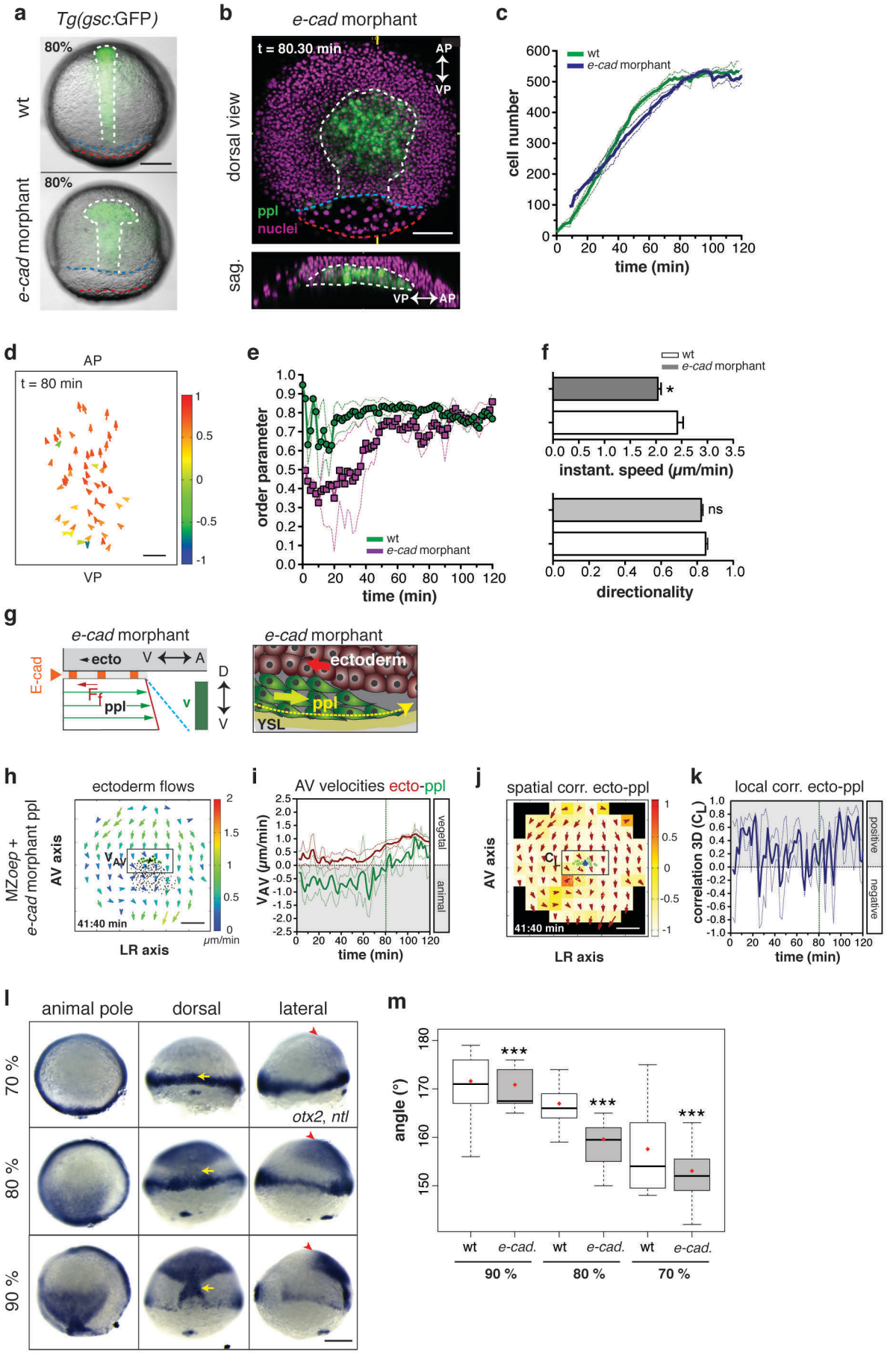

Supplementary Figure-8, Heisenberg